Cellular and Molecular Biology
E-ISSN : 1165-158X / P-ISSN : 0145-5680
www.cellmolbiol.org

CircBCAR3 sponges miR-27a-3p and mediates ferroptosis in human B-prolymphocytic leukaemia cells via SLC7A11

Guangwei Zhao[1#], Huan Chen[2#], Jianmin Luo[3*]

[1] Department of Oncology, The Second Hospital of Hebei Medical University, Shijiazhuang, China
[2] Department of Ophthalmology, The Second Hospital of Hebei Medical University, Shijiazhuang, China
[3] Department of Hematopathology, The Second Hospital of Hebei Medical University, Shijiazhuang, China

[#] Guangwei Zhao and Huan Chen contributed equally to this work.

ARTICLE INFO

Original paper

Article history:
Received: June 12, 2023
Accepted: September 12, 2023
Published: November 30, 2023

Keywords:

CircBCAR3, miR-27a-3p, SLC7A11, ferroptosis, B-prolymphocytic leukaemia

ABSTRACT

B-lymphocytic leukaemia is one of the most commonly diagnosed blood malignancies, and our knowledge of B-prolymphocytic leukaemia remained barely comprehensive. CircRNAs and miRNAs were identified as important regulatory roles in tumours. This study focused on the possibly existing interaction of circBCAR3 and miR-27a-3p, and downstream molecules thereafter in B-prolymphocytic leukaemia cells. CircBCAR3 and miR-27a-3p expression were evaluated in JVM-2 cell line and normal lymphocytes. Dual-luciferase luminescence assay was conducted for validation of circBCAR3 and miR-27a-3p interaction, as well as western blot and flow cytometry for evaluation and validation of their association with SLC7A11, reactive-oxygen species and Fe^{2+} regarding ferroptosis. CircBCAR3 was upregulated in JVM-2 cells and was reversely correlated with the expression of miR-27a-3p. CircBCAR3 targeted at miR-27a-3p and was consequently associated with SLC7A11 expression positively, inhibiting ferroptosis and peroxidative damage in JVM-2 cells. This study identified a circBCAR3-miR-27a-3p-SLC7A11 axis regulating ferroptosis and peroxidation of B-prolymphocytic leukaemia cells which might be a key mechanism facilitating the survival of tumour cells. However, further validation based on more diverse cell lines and animal models might be required.

Doi: http://dx.doi.org/10.14715/cmb/2023.69.12.29 Copyright: © 2023 by the C.M.B. Association. All rights reserved.

Introduction

B-lymphocytic leukaemia is regarded as one of the most commonly diagnosed types of blood cancer malignancies, and also has it been one of the most developing realms of medical scientific research in the past years (1, 2). B-prolymphocytic leukaemia (B-PLL) is considered to be a specific type of blood cancer malignancy first formally reported by Galton's team in 1974 based on an observation and summarisation of the condition of 15 patients diagnosed with a variant of chronic lymphocytic leukaemia of a remarkably low incidence (3). According to currently available statistical data, the proportion of B-PLL barely gets more than 1% of all lymphocytic leukaemia cases, and is still in need of further study into the depth mechanically and clinically (4-6). Current common consensus demonstrates that B-PLL is most often diagnosed among aged patients with the features of high white blood cell counts, a large proportion of prolymphocytes, as well as relatively severe splenomegaly yet mild or no lymphadenopathy (7). Although some might display a relatively longer overall survival, the prognosis of the majority of patients diagnosed with B-PLL remains unfavourably poor (7, 8). TP53, MYC, as well as a variety of other targets, have been identified and utilised as therapeutic targets and have been confirmed to be of observable efficacy in some studies, yet better insights into the mechanisms and potential targets are still expected (4, 9-12).

The human genome consists of approximately 6.4 billion base pairs and it is believed that three-quarters of them are undergoing active transcription. However, currently available data revealed that nearly 98% of the RNAs transcribed encoded no protein at all, and are therefore regarded as non-coding RNAs (13). Non-coding RNAs can be further classified into a diversity of subgroups like ribosomal RNA (rRNA), transfer RNA (tRNA), micro-RNA (miRNA/miR), circular RNA (circRNA), etc. (14,15). Enormous quantities of investigations into non-coding RNAs were conducted accordingly, demonstrating a magnificent diversity of regulatory functions regarding the processing of RNAs and the expression of genes (13), and thus dysfunction of those RNAs would result in a malfunction of gene expression, which might then lead to disorders in cytological regulation and even contribute to the initiation and progression of tumours. As a loop-shaped subtype of non-coding RNA synthesised via back splicing, circRNA has been confirmed to participate in ranges of cytological and tumorigenic procedures like cell proliferation, apoptosis, tumour invasion and migration (16-18). miRNA is another well-studied non-coding RNA targeting specific mRNAs in a complementary manner, either hampering further translation or facilitating further degradation of the mRNA (19-21). Sufficient evidences demonstrated the interactive association between circRNA and

* Corresponding author. Email: luojm3155@163.com

miRNA, claiming a sponge-like role of circRNA that one circRNA was capable of binding multiple or even quantities of specific types of miRNAs, impeding the exertion of inhibitory function of miRNAs in mRNA translation and consequently enhancing the expression of specific clusters of genes (22-26). Accumulating studies have indicated the involvement of such mechanism in the initiation and development of a wide range of tumours (26-32). However, few studies placed their focus on such mechanism in the realm of the relatively rare disease, B-PLL, which turned to be a blank waiting for filling in.

It is therefore the purpose of this study to explore the possibly existing mechanism consisting of circBCAR3 and miR-27a-3p in the initiation and development of B-PLL, seeking to fill in the blank that currently exists.

Materials and Methods

Cell Culture

Human embryonic kidney cell line 293T and human B-prolymphocytic leukaemia isolated cell line JVM-2 were acquired from American Tissue Culture Collection (ATCC, Rockville, MD, USA), human normal B lymphocyte was acquired from BeNa Culture Collection (BNCC, Henan, China).

293T cells were cultured in DMEM medium (D0819, GIBCO, Invitrogen Corporation, NY, USA) with 100 U/mL penicillin & 100 μg/mL streptomycin (15140148) (Thermo Fisher Scientific, Pittsburgh, PA, USA), 2 mM L-glutamine (30-2214) (ATCC) and 10% FBS (SH30070.03) (FBS, Hyclone, Logan, UT, USA). JVM-2 cells and human B lymphocytes were cultured in RPMI-1640 medium (A33823, GIBCO, Invitrogen Corporation, NY, USA) with 100 U/mL penicillin & 100 μg/mL streptomycin and 10% FBS. Cells were cultured at 37 °C/5% CO2 and medium was replaced with fresh medium once every 2 days. Subculture of all the 3 different types of cells took place when approximately 90% percent of the plate surface was covered.

Cell Transfection

Cells were seeded in 24-well plates one day before transfection with penicillin/streptomycin-free medium. siRNAs (si-NC and si-circBCAR3) and miRNA mimics (mimics-NC and miR-27a-3p mimics) were resolved with Opti-MEM medium (31985062, GIBCO, Invitrogen Corporation, NY, USA) and lipo 3000 (L3000150, Thermo Fisher Scientific, Pittsburgh, PA, USA). Cells were cultured with transfection mixture for 15 min and Opti-MEM afterwards. Opti-MEM was replaced by maximal medium 6 h after transfection and cells were harvested after 24 h for further experiments. Quantitative real-time polymerase chain reaction (qRT-PCR) was conducted for validation of transfection efficiency.

Dual luciferase luminescence Assay

Dual luciferase luminescence assay was conducted via Dual Luciferase Reporter Gene Assay Kit (RG028, Beyotime, Shanghai, China) in accordance with the protocol provided by the manufacturer. In short terms, cells were pre-seeded in 24-well plates and were transfected with dual luciferase luminescence reporter vector pre-constructed (detailed information regarding the construction of reporter vector can be found in Supplementary Section 1) via lipo 3000 and Opti-MEM in similar manners as described in Cell Transfection section. Cells were afterwards harvested and lysed followed by centrifugation at 10000~15000RPM for 3~5min to obtain the supernatant. Luciferase detection reagent was then added and the signal was detected via Berthold Technologies™ TriStar LB 941.

Western Blot Assay

Cells were seeded in 6-well plates and were harvested when 90% of the culture surface was covered. The total protein of cells was extracted by cell lysis via PMSF (Amresco, Solon, OH, USA) containing RIPA (Beyotime, Shanghai, China) and ultracentrifugation with the obtaining of the supernatant.

Samples were then separated via 10~12% SDS-PAGE (Amresco, Solon, OH, USA) and transferred to PVDF membranes (Millipore, Schwalbach, Germany). 5% skim milk TBST solution was used for membrane blocking for 1h under room temperature followed by incubation of antibodies consecutively. All antibodies used in this study were purchased from Abcam (Abcam, Cambridge, UK).

qRT-PCR Assay

Cells were seeded in 6-well plates and were harvested when 90% of the culture surface was covered. mRNAs were extracted from cells via TRIzol (9109, TaKaRa, Tokyo, Japan) and miRNAs were extracted from cells via an miRNA extraction kit (B1802, Haigene, Harbin, China). Complementary DNAs (cDNAs) of mRNAs were reversely transcribed via iScript cDNA synthesis kit (1708891EDU, Bio-Rad, Hercule, USA) and cDNAs of miRNAs were reversely transcribed via one-step miRNA reverse transcription kit (D1801, Haigene, Harbin, China) according to the protocol provided by the manufacturer. Applied Biosystems™ 7500 Real-Time PCR Instrument was used for the conduct of qPCR assay. All primers used in this study were provided by Sangon Biotech (Sangon Biotech, Shanghai, China), primer sequences were listed as follows: circBCAR2, forward: 5'-CCTGGAAACAGCAATGTTGA-3', reverse: 5'-GTCCATGATGTGCCTCTCCT-3'; GAPDH, forward: 5'-AATGGGCAGCCGTTAGGAAA-3', reverse: 5'-GCGCCCAATACGACCAAATC-3'; miR-27a-3p, forward: 5'-TGCGGTTCACAGTGGCTAAG-3', reverse: 5'-CTCAACTGGTGTCGTGGA-3'; U6, forward: 5'-CTCGCTTCGGCAGCACA-3', reverse: 5'-AACGCTTCACGAATTTGCGT-3'.

Cell Viability Validation

The viability of cells was validated via MTT assay using MTT assay kit (C0009S, Beyotime, Shanghai, China) in accordance with the protocol provided by the manufacturer. Briefly, cells were pre-seeded in 96-well plates and the medium was replaced by FBS-free medium when 80% of the culture surface was covered. Cells were incubated in FBS free medium for 2 h before switching back to maximal medium for another 24 h's incubation. MTT was added at the 20th hour of incubation and the medium was replaced by DMSO after incubation. OD_{570} was measured via Berthold Technologies™ TriStar LB 941 for the detection of cell viability.

Cell Apoptosis Validation

The apoptosis of cells was validated using Annexin V-FITC/PI Cell Apoptosis Kit (KGA108-1, KeyGEN,

Nanjing, China) according to manufacturer's protocol. To be brief, cells were harvested, washed and resuspended by Binding Buffer followed by the addition of Annexin V-FITC resolution and Propidium Iodide for 15 min's light avoided incubation. Cells were afterwards measured and analysed via Beckman™ DxFlex flow cytometry instrument within 1h.

Cell Reactive Oxygen Species (ROS) Detection

The ROS within cells was detected using ROS detection kit (S0033S, Beyotime, Shanghai, China) in accordance with the protocol provided by the manufacturer. Briefly speaking, the DCFH-DA prob (S0063, Beyotime, Shanghai, China) was diluted at the ratio of 1:1000 and was then used for the resuspension of harvested cells. The resuspension was then incubated away from lights for 20min followed by fluorescence detection at 525 nm via Beckman™ DxFlex flow cytometry instrument.

Cell Fe^{2+} Detection

Cells were harvested, washed and resuspended in PBS followed by the addition of FerroOrange Fe^{2+} prob (MX4559-48UG, MKBio, Shanghai, China) and light-avoided incubation for 30min under room temperature. Cells were afterwards washed, resuspended and the fluorescence was detected via Beckman™ DxFlex flow cytometry instrument.

Cell Glutathione (reduced form) (GSH) Detection

The cytosol GSH level was detected via the GSH detection kit (ml094982, MIBio, Shanghai, China) in accordance with the protocol provided by the manufacturer. In simple terms, cells were harvested, washed with PBS and resuspended with GSH extractor resolution. Resuspension was then treated by rapid freeze-thaw and was incubated on ice for 5 min followed by centrifugation at 12000RPM. The supernatant was collected and pre-prepared DTNB resolution was added for further reaction at 10 min under 25 degrees Celsius. OD_{412} was measured via Berthold Technologies™ TriStar LB 941 for the detection of GSH concentration.

Statistical analysis

Analysation, illustration and interpretation of data were conducted based on Graphpad Prism 9 (version 9.4.0) and Adobe Illustrator 2022 (version 2022). All quantitative data were described as means ± standard deviation, and intergroup statistical differences were validated via one-way ANOVA and Tukey's test, with a statistically significant difference identified if $P<0.05$ was confirmed.

Results

CircBCAR3 was upregulated in lymphocytic leukaemia cell line JVM-2

For the purpose of a clear illustration of the expression alteration of circBCAR3 in B-prolymphocytic leukaemia, qRT-PCR was conducted for evaluation of the circBCAR3 expression in normal B lymphocytes and JVM-2 cells to reveal a significant abnormal upregulation of circBCAR3 expression in JVM-2 cells as compared with normal B lymphocytes (Figure 1).

CircBCAR3 targeted at miR-27a-3p in lymphocytic leukaemia cell line JVM-2

As predicted via analysation of data stored in the ENCORI database for screening of the potentially existing miRNAs having the capacity of binding to circBCAR3, miR-27a-3p was identified to be of a relatively high rank with a targeted binding association. Also had a targeted binding association has been identified via ENCORI data analysation between miR-27a-3p and SCL7A11, with supportive evidence provided in previous investigations based on dual-luciferase assay (33). Given such, a dual luciferase assay was conducted in this study for the purpose of verification of the targeted binding of circBCAR3 to miR-27a-3p. By construction and transfection of wild-type circBCAR3 (circBCAR3-WT) and mutated circBCAR3 dual luciferase vector (circBCAR3-MUT), results yielded by the assay demonstrated that circBCAR3 bound to miR-27a-3p in a targeted manner via multiple sites as illustrated in Figure 2.

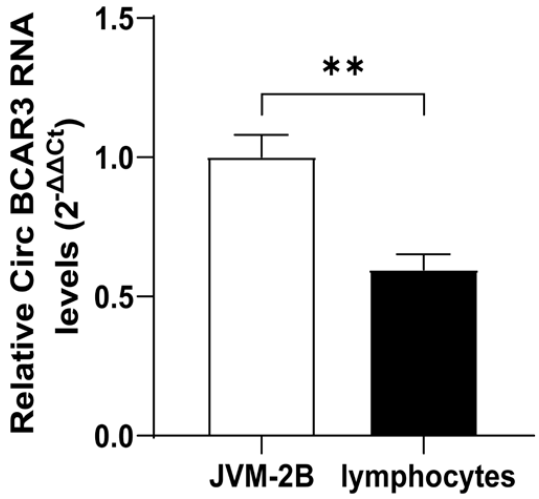

Figure 1. The RNA levels of circBCAR3 were measured by qRT-PCR. Results were mean ± SD for three individual experiments. **P<0.01.

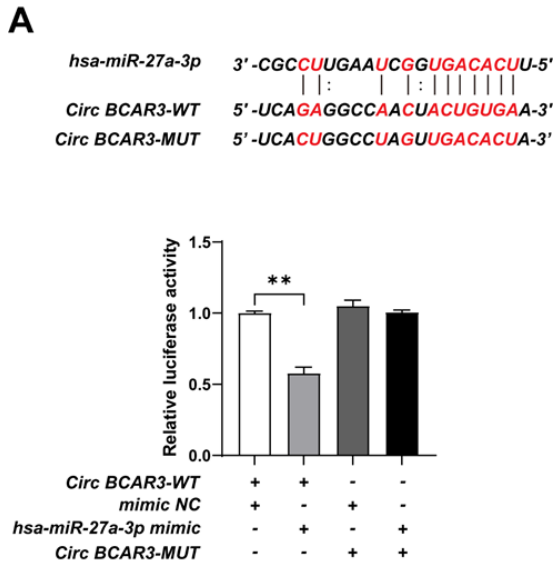

Figure 2. hsa-miR-27a-3p can bind to circBCAR3. After 293T cells were co-transfected with circBCAR3 luciferase report vector (circBCAR3-WT, circBCAR3-MUT) and mimics-NC, hsa-miR-27a-3p mimic (A), the luciferase signal was determined. Results were mean ± SD for three individual experiments. *P<0.05, **P<0.01.

CircBCAR3 interference suppressed cell viability and promoted apoptosis

Enhanced cell apoptosis and decreased cell viability were observed in JVM-2 cells transfected with miR-27a-3p mimics as compared to those transfected with mimics NC (negative control), and similar phenomenon was also observed in JVM-2 cells transfected with si-circBCAR3, a siRNA designed for knocking down of the circBCAR3 expression, as compared to those transfected with siRNA-NC. Furthermore, double transfection of both si-circBCAR3 and miR-27a-3p mimics was observed to result in an even more significant suppression of cell viability and an even significant promotion of cell apoptosis, as illustrated in Figure 3.

Expression of circBCAR3 negatively correlated with the expression of miR-27a-3p

JVM-2 cells were transfected with miR-27a-3p mimics (and mimics NC as negative control) and/or si-circBCAR3 (and siRNA-NC as negative control) for interventional upregulation of the corresponding molecules and the expression of the molecules were validated via qRT-PCR. As demonstrated by the results, significant upregulation of miR-27a-3p could be observed not only in miR-27a-3p mimics transfected cells, but in si-circBCAR3 transfected cells as well, and even greater upregulation of its expression was observed in cells undergone double transfection (Figure 4A). Consistently, significant downregulation of circBCAR3 could be observed not only in si-circBCAR3 transfected cells, but in miR-27a-3p transfected cells as well, and an even greater downregulation was observed in cells undergoing double transfection (Figure 4B).

Expression of SLC7A11 co-altered with the expression of circBCAR3 and miR-27a-3p

It has been demonstrated by previous studies that SLC7A11 binds to miR-27a-3p in a targeted manner (33) and it has been demonstrated in the former section of this study that circBCAR3 bounded to miR-27a-3p in a targeted manner. Given such, western blot assay was conducted for the validation of SLC7A11 expression in JVM-2 cells differently treated as described in the former section. According to the results, significant downregulation of SLC7A11 expression could be observed in cells either transfected with miR-27a-3p mimics (in which miR-27a-3p was significantly upregulated) or with si-circBCAR3 (in which circBCAR3 was significantly downregulated), and an even greater downregulation can be observed in cells undergone double transfection (Figure 5).

CircBCAR3 reduced cytosol GSH and increased the concentration of ROS and Fe^{2+}

The former sections of this study enlightened an indication of the existence of a cell regulatory axis of circBCAR3-miR-27a-3p-SLC7A11. Previous studies have demonstrated profoundly validated inhibitory function of SLC7A11 in the peroxidative damage caused by ferroptosis (34-37). Taken together, it was hypothesised in this study that the circBCAR3-miR-27a-3p-SLC7A11 regulatory axis could exert similar inhibition upon ferroptosis-induced peroxidative damage to JVM-2 cells, and consequently, suppression of such axis could restore ferroptosis induced peroxidation. For validation of the hypothesis, Fe^{2+}, ROS and GSH in JVM-2 cells undergoing

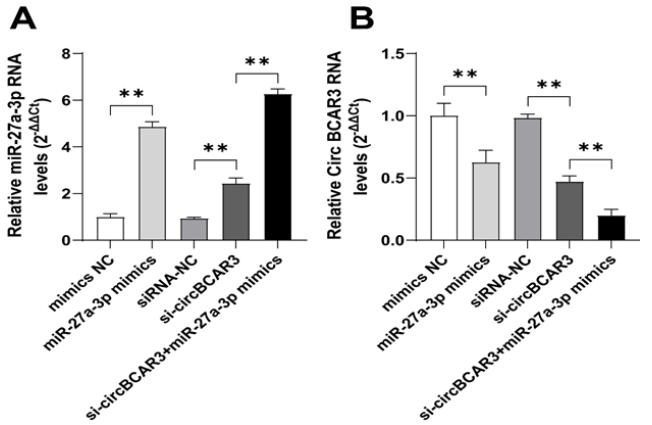

Figure 4. The expression of miR-27a-3p overexpression or circBCAR3 knockdown on JVM-2 cells. JVM-2 cells were transfected with mimics NC, miR-27a-3p mimics, siRNA-NC, si- cicBCAR3 and si-cicBCAR3+ miR-27a-3p mimics. The RNA levels of miR-27a-3p (A) and circBCAR3 (B) were measured by qRT-PCR. Results were mean ± SD for three individual experiments. *P<0.05, **P<0.01.

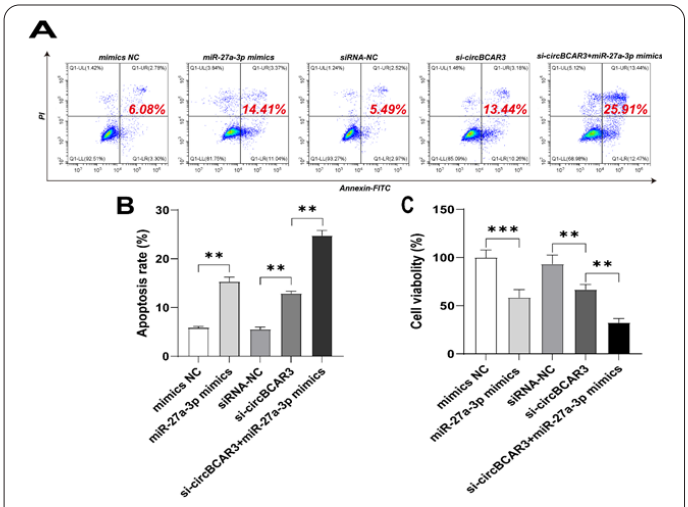

Figure 3. The expression of miR-27a-3p overexpression or cicBCAR3 knockdown on JVM-2 cells. JVM-2 cells were transfected with mimics NC, miR-27a-3p mimics, siRNA-NC, si- cicBCAR3 and si-cicBCAR3+ miR-27a-3p mimics. The apoptosis (A, B) ratio of JVM-2 cells in the indicated group was measured by flow cytometric analysis. The cell viability (C) was detected by MTT assay. Results were mean ± SD for three individual experiments. *P<0.05, **P<0.01.

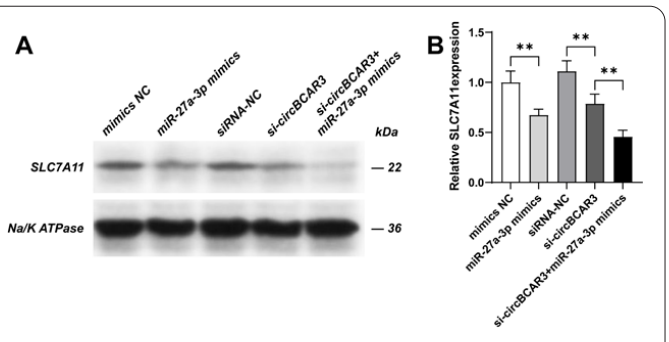

Figure 5. The expression of miR-27a-3p overexpression or circBCAR3 knockdown on JVM-2 cells. JVM-2 cells were transfected with mimics NC, miR-27a-3p mimics, siRNA-NC, si- cicBCAR3 and si- cicBCAR3+ miR-27a-3p mimics. The expression of SLC7A11 (A, B) from the indicated group was detected by western blot assay. Results were mean ± SD for three individual experiments. *P<0.05, **P<0.01.

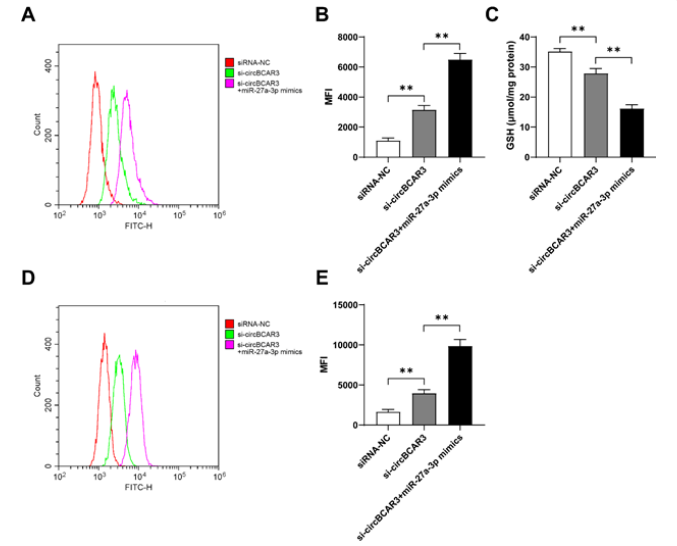

Figure 6. The expression of miR-27a-3p overexpression or circBCAR3 knockdown on JVM-2 cells. JVM-2 cells were transfected with siRNA-NC, si-cicBCAR3 and si-cicBCAR3+ miR-27a-3p mimics. ROS level (DCFH-DA probe) (A, B) in JVM-2 cells was detected by flow cytometry. The expression of GSH (C) was detected by GSH assay kits. The levels of Fe2+ were detected by flow cytometry (D, E). Results were mean ± SD for three individual experiments. *P<0.05, **P<0.01.

different interventions were detected and measured. As demonstrated by the outcome of the experiments, Fe^{2+} and ROS were significantly increased in JVM-2 cells transfected with circBCAR3 while GSH was significantly reduced, as compared to negative control. Consistently, a similar phenomenon was observed also in JVM-2 cells transfected with miR-27a-3p mimics as compared to negative control. Even greater increments of Fe^{2+} and ROS and a decrease in GSH were observed in JVM-2 cells undergoing double transfection. Such results were considered to be positive support for the hypothesis of the existence of circBCAR3-miR-27a-3p-SLC7A11 axis in B-prolymphocytic leukaemia cell line JVM-2 (Figure 6).

Discussion

B-PLL, although discovered, formally documented and reported as early as 1974, remained less well studied till nowadays (3, 4, 9-12). Various targets including TP53 and MYC have been identified and utilised for therapeutic purposes with some observable efficacy, yet the majority of the patient diagnosed with B-PLL remained unfavourably poor, which calls for better insights into the mechanisms of B-PLL (7, 8).

The role of non-coding RNAs, especially circRNAs and miRNAs, is now gaining growing attention and being profoundly investigated in recent decades. miRNAs are sequence-specific mRNA inhibitors that can bind to mRNAs complementarily for hampering translation and/or facilitating degradation (19-21), which in other terms indicates that miRNAs can act either tumour promotively or tumour suppressively depending on the genetic messages on which mRNAs targeted would be carrying or in which type of cells would the miRNAs be functioning. Previous studies claimed that some miRNAs like miR-141, miR-21, miR-30b-5p and miR-1304-3p function promotively in the initiation and development of malignancies (38-41) while some others like miR-155, miR-4516, miR-340-5p and miR-489 function suppressively (42-45).

Similarly, the role of circRNAs in tumours is also diverse and relatively complicated yet the mechanisms of their functions can be briefly summarised as the following 3: a. inhibiting the miRNA function via sponging; b. interacting with proteins in sponge-like or scaffold-like manners and thus suppressing further translation of specific proteins, facilitating enzymatic catalysation or recruiting specific factors to specific sites; c. a small proportion of circRNAs bear the capability of acting as templates for proteins or peptides translation, which is a function same as mRNAs (46-50). CircRNAs have been demonstrated participating in wide ranges of cytological and tumorigenic procedures (15-18), including the initiation and development of glioma, hepatocellular carcinoma, breast cancer, colon cancer, etc. (51-54), and, similar to the effect of miRNAs, the overall effect of circRNAs on the initiation and development of tumours differs, some like circACTN4, circWSB1, circMTCL1 and circRHOT1 function promotively (50, 55-57) while some like circDIDO1, circPTEN1, circMRPS35 and circEIF4G3 function suppressively (58-61).

Last year, Yong Xi et al. proposed their discovery that circBCAR3 exhibited the capacity of oesophageal malignancy development acceleration through interaction with miR-27a-3p in a sponge-like manner which would consequently upregulate the expression of transportin-1 (TNPO-1) (26). The year before last year, Xuan Lu et al. proposed their finding of the interaction between miR-27a-3p and SLC7A11 (33). Now, this study demonstrates the existence of a circBCAR3-miR-27a-3p-SLC7A11 axis as an inhibitory mechanism in the process of ferroptosis and consequently as a promotive mechanism in the survival of B-PLL cells.

Together, it is of optimistic perspective that this newly discovered circBCAR3-miR-27a-3p-SLC7A11 axis in B-PLL cells might be one of the key mechanisms supporting tumorigenesis and thus might have the potential of being a candidate target for utilisation of targeted therapy in B-PLL patients. Further exploration of this axis in tumours of other origins might be required, as well as more solid validations of this axis based on more lymphocytic cell lines and animal models.

Ethical Compliance

Not applicable.

Conflict of Interests

The authors declared no conflict of interest.

Acknowledgments

This study did not receive any funding in any form

References

1. Hallek M, Shanafelt TD, Eichhorst B. Chronic lymphocytic leukaemia. Lancet 2018; 391(10129): 1524-1537.
2. Luo X, Zhang Y, Chen Q. Nursing Care Plan and Management of Patients With Acute Leukemia. Altern Ther Health M 2022; 28(1): 80-85.
3. Feng Y, Su B, Xu Y, He Y, He R, Ge F. Expression of CD123 related long non-coding RNA in Acute Myeloid Leukemia bone marrow mononuclear cells and its clinical significance. Cell Mol

Biol 2022; 68(6): 140-147.
4. Xing L, He Q, Xie L, Wang H, Li Z. Zanubrutinib, rituximab and lenalidomide induces deep and durable remission in TP53-mutated B-cell prolymphocytic leukemia: a case report and literature review. Haematologica 2022; 107(5): 1226-1228.
5. Collignon A, Wanquet A, Maitre E, Cornet E, Troussard X, Aurran-Schleinitz T. Prolymphocytic Leukemia: New Insights in Diagnosis and in Treatment. Curr Oncol Rep 2017; 19(4): 29.
6. Swerdlow SH, Campo E, Pileri SA, et al. The 2016 revision of the World Health Organization classification of lymphoid neoplasms. Blood 2016; 127(20): 2375-2390.
7. van der Velden VH, Hoogeveen PG, de Ridder D, et al. B-cell prolymphocytic leukemia: a specific subgroup of mantle cell lymphoma. Blood 2014; 124(3): 412-419.
8. Dearden C. How I treat prolymphocytic leukemia. Blood 2012; 120(3): 538-551.
9. Abd El-Lateef AE, Ismail MM, Almohammadi M, Gawaly AM. Prognostic relevance of combined IDH1 and NPM1 mutations in the intermediate cytogenetic de novo acute myeloid leukemia. Cell Mol Biol 2021; 67(3): 92-98.
10. Eyre TA, Fox CP, Boden A, et al. Idelalisib-rituximab induces durable remissions in TP53 disrupted B-PLL but results in significant toxicity: updated results of the UK-wide compassionate use programme. Brit J Haematol 2019; 184(4): 667-671.
11. Gordon MJ, Raess PW, Young K, Spurgeon S, Danilov AV. Ibrutinib is an effective treatment for B-cell prolymphocytic leukaemia. Brit J Haematol 2017; 179(3): 501-503.
12. Zhao L, Liu D, Zhong C, et al. Evaluating the role of Ubiquitin D gene expression in types of leukemia br. Cell Mol Biol 2022; 68(9): 125-128.
13. Decoding noncoding RNAs. Nat Methods 2022; 19(10): 1147-1148.
14. Seal RL, Chen LL, Griffiths-Jones S, et al. A guide to naming human non-coding RNA genes. Embo J 2020; 39(6): e103777.
15. Yang L, Ma T, Zhang Y, Wang H, An R. Construction and Analysis of lncRNA-miRNAmRNA ceRNA Network Identify an Eight-Gene Signature as a Potential Prognostic Factor in Kidney Renal Papillary Cell Carcinoma (KIRP). Altern Ther Health M 2022; 28(6): 42-51.
16. Sang Y, Chen B, Song X, et al. circRNA_0025202 Regulates Tamoxifen Sensitivity and Tumor Progression via Regulating the miR-182-5p/FOXO3a Axis in Breast Cancer. Mol Ther 2019; 27(9): 1638-1652.
17. Yang H, Zhang H, Yang Y, et al. Hypoxia induced exosomal circRNA promotes metastasis of Colorectal Cancer via targeting GEF-H1/RhoA axis. Theranostics 2020; 10(18): 8211-8226.
18. Yang Q, Li F, He AT, Yang BB. Circular RNAs: Expression, localization, and therapeutic potentials. Mol Ther 2021; 29(5): 1683-1702.
19. Rupaimoole R, Slack FJ. MicroRNA therapeutics: towards a new era for the management of cancer and other diseases. Nat Rev Drug Discov 2017; 16(3): 203-222.
20. Du T, Zamore PD. Beginning to understand microRNA function. Cell Res 2007; 17(8): 661-663.
21. O'Connell RM, Zhao JL, Rao DS. MicroRNA function in myeloid biology. Blood 2011; 118(11): 2960-2969.
22. Denzler R, Agarwal V, Stefano J, Bartel DP, Stoffel M. Assessing the ceRNA hypothesis with quantitative measurements of miRNA and target abundance. Mol Cell 2014; 54(5): 766-776.
23. Hansen TB, Jensen TI, Clausen BH, et al. Natural RNA circles function as efficient microRNA sponges. Nature 2013; 495(7441): 384-388.
24. Poliseno L, Salmena L, Zhang J, Carver B, Haveman WJ, Pandolfi PP. A coding-independent function of gene and pseudogene mRNAs regulates tumour biology. Nature 2010; 465(7301): 1033-1038.
25. Salmena L, Poliseno L, Tay Y, Kats L, Pandolfi PP. A ceRNA hypothesis: the Rosetta Stone of a hidden RNA language? Cell 2011; 146(3): 353-358.
26. Xi Y, Shen Y, Wu D, et al. CircBCAR3 accelerates esophageal cancer tumorigenesis and metastasis via sponging miR-27a-3p. Mol Cancer 2022; 21(1): 145.
27. Cui X, Wang J, Guo Z, et al. Emerging function and potential diagnostic value of circular RNAs in cancer. Mol Cancer 2018; 17(1): 123.
28. Dong W, Bi J, Liu H, et al. Circular RNA ACVR2A suppresses bladder cancer cells proliferation and metastasis through miR-626/EYA4 axis. Mol Cancer 2019; 18(1): 95.
29. Peng QS, Cheng YN, Zhang WB, Fan H, Mao QH, Xu P. circRNA_0000140 suppresses oral squamous cell carcinoma growth and metastasis by targeting miR-31 to inhibit Hippo signaling pathway. Cell Death Dis 2020; 11(2): 112.
30. Shang Q, Yang Z, Jia R, Ge S. The novel roles of circRNAs in human cancer. Mol Cancer 2019; 18(1): 6.
31. Shi Y, Fang N, Li Y, et al. Circular RNA LPAR3 sponges microRNA-198 to facilitate esophageal cancer migration, invasion, and metastasis. Cancer Sci 2020; 111(8): 2824-2836.
32. Zhong Y, Du Y, Yang X, et al. Circular RNAs function as ceRNAs to regulate and control human cancer progression. Mol Cancer 2018; 17(1): 79.
33. Lu X, Kang N, Ling X, Pan M, Du W, Gao S. MiR-27a-3p Promotes Non-Small Cell Lung Cancer Through SLC7A11-Mediated-Ferroptosis. Front Oncol 2021; 11: 759346.
34. Badgley MA, Kremer DM, Maurer HC, et al. Cysteine depletion induces pancreatic tumor ferroptosis in mice. Science 2020; 368(6486): 85-89.
35. He F, Zhang P, Liu J, et al. ATF4 suppresses hepatocarcinogenesis by inducing SLC7A11 (xCT) to block stress-related ferroptosis. J Hepatol 2023; 79(2): 362-377.
36. Lei G, Zhang Y, Koppula P, et al. The role of ferroptosis in ionizing radiation-induced cell death and tumor suppression. Cell Res 2020; 30(2): 146-162.
37. Yang M, Wu X, Hu J, et al. COMMD10 inhibits HIF1alpha/CP loop to enhance ferroptosis and radiosensitivity by disrupting Cu-Fe balance in hepatocellular carcinoma. J Hepatol 2022; 76(5): 1138-1150.
38. Chen K, Wang Q, Liu X, Wang F, Yang Y, Tian X. Hypoxic pancreatic cancer derived exosomal miR-30b-5p promotes tumor angiogenesis by inhibiting GJA1 expression. Int J Biol Sci 2022; 18(3): 1220-1237.
39. Hashemi M, Mirdamadi M, Talebi Y, et al. Pre-clinical and clinical importance of miR-21 in human cancers: Tumorigenesis, therapy response, delivery approaches and targeting agents. Pharmacol Res 2023; 187: 106568.
40. Mo Y, Leung LL, Mak C, et al. Tumor-secreted exosomal miR-141 activates tumor-stroma interactions and controls premetastatic niche formation in ovarian cancer metastasis. Mol Cancer 2023; 22(1): 4.
41. Zhao D, Wu K, Sharma S, et al. Exosomal miR-1304-3p promotes breast cancer progression in African Americans by activating cancer-associated adipocytes. Nat Commun 2022; 13(1): 7734.
42. Chen S, Xu M, Zhao J, et al. MicroRNA-4516 suppresses pancreatic cancer development via negatively regulating orthodenticle homeobox 1. Int J Biol Sci 2020; 16(12): 2159-2169.
43. Lu G, Zhang Y. MicroRNA-340-5p suppresses non-small cell lung cancer cell growth and metastasis by targeting ZNF503. Cell Mol Biol Lett 2019; 24: 34.
44. Paskeh M, Mirzaei S, Orouei S, et al. Revealing the role of miR-

NA-489 as a new onco-suppressor factor in different cancers based on pre-clinical and clinical evidence. Int J Biol Macromol 2021; 191: 727-737.
45. Wang J, Wang Q, Guan Y, et al. Breast cancer cell-derived microRNA-155 suppresses tumor progression via enhancing immune cell recruitment and antitumor function. J Clin Invest 2022; 132(19): e157248.
46. Abdelmohsen K, Panda AC, Munk R, et al. Identification of HuR target circular RNAs uncovers suppression of PABPN1 translation by CircPABPN1. RNA Biol 2017; 14(3): 361-369.
47. Jarlstad OM, S KL. Circular RNAs as microRNA sponges: evidence and controversies. Essays Biochem 2021; 65(4): 685-696.
48. Lei M, Zheng G, Ning Q, Zheng J, Dong D. Translation and functional roles of circular RNAs in human cancer. Mol Cancer 2020; 19(1): 30.
49. Li B, Zhu L, Lu C, et al. circNDUFB2 inhibits non-small cell lung cancer progression via destabilizing IGF2BPs and activating anti-tumor immunity. Nat Commun 2021; 12(1): 295.
50. Wang L, Long H, Zheng Q, Bo X, Xiao X, Li B. Circular RNA circRHOT1 promotes hepatocellular carcinoma progression by initiation of NR2F6 expression. Mol Cancer 2019; 18(1): 119.
51. Li X, Wang J, Lin W, et al. circEXOC6B interacting with RRAGB, an mTORC1 activator, inhibits the progression of colorectal cancer by antagonizing the HIF1A-RRAGB-mTORC1 positive feedback loop. Mol Cancer 2022; 21(1): 135.
52. Yi J, Wang L, Hu GS, et al. CircPVT1 promotes ER-positive breast tumorigenesis and drug resistance by targeting ESR1 and MAVS. Embo J 2023; 42(10): e112408.
53. Zhang M, Huang N, Yang X, et al. A novel protein encoded by the circular form of the SHPRH gene suppresses glioma tumorigenesis. Oncogene 2018; 37(13): 1805-1814.
54. Zhang X, Qiu S, Luo P, et al. Down-regulation of hsa_circ_0001649 in hepatocellular carcinoma predicts a poor prognosis. Cancer Biomark 2018; 22(1): 135-142.
55. Wang X, Xing L, Yang R, et al. The circACTN4 interacts with FUBP1 to promote tumorigenesis and progression of breast cancer by regulating the expression of proto-oncogene MYC. Mol Cancer 2021; 20(1): 91.
56. Wang Z, Sun A, Yan A, et al. Circular RNA MTCL1 promotes advanced laryngeal squamous cell carcinoma progression by inhibiting C1QBP ubiquitin degradation and mediating beta-catenin activation. Mol Cancer 2022; 21(1): 92.
57. Yang R, Chen H, Xing L, et al. Hypoxia-induced circWSB1 promotes breast cancer progression through destabilizing p53 by interacting with USP10. Mol Cancer 2022; 21(1): 88.
58. Jie M, Wu Y, Gao M, et al. CircMRPS35 suppresses gastric cancer progression via recruiting KAT7 to govern histone modification. Mol Cancer 2020; 19(1): 56.
59. Zang X, Jiang J, Gu J, et al. Circular RNA EIF4G3 suppresses gastric cancer progression through inhibition of beta-catenin by promoting delta-catenin ubiquitin degradation and upregulating SIK1. Mol Cancer 2022; 21(1): 141.
60. Zhang Y, Jiang J, Zhang J, et al. CircDIDO1 inhibits gastric cancer progression by encoding a novel DIDO1-529aa protein and regulating PRDX2 protein stability. Mol Cancer 2021; 20(1): 101.
61. Zheng L, Liang H, Zhang Q, et al. circPTEN1, a circular RNA generated from PTEN, suppresses cancer progression through inhibition of TGF-beta/Smad signaling. Mol Cancer 2022; 21(1): 41.